Resistance Spot Welding of Dissimilar Interstitial-Free and High-Strength Low-Alloy Steels

Gorti Janardhan, Goutam Mukhopadhyay, Kaushal Kishore, and Krishna Dutta

The primary aim of this investigation is to examine the resistance spot weldability of dissimilar interstitial-free (IF) and high-strength low-alloy (HSLA) steels. The effect of dynamic contact resistance on the nugget diameter is examined. The mechanical properties of the spot-welded specimens are investigated in both tensile shear and coach peel configurations. These experiments are supplemented by macro- and microstructural examinations, determination of microhardness profiles, and post-failure examinations, including fractography. It is observed that the nugget diameter increases as mean dynamic contact resistance decreases. The heat-affected zone of the HSLA side of the weld joint shows the maximum hardness, whereas the base metal of the IF side shows the minimum hardness. The hardness at the fusion zone of the dissimilar HSLA–IF joint lies in between that of fusion zone of similar HSLA–HSLA and IF–IF joints because of the homogenization of the chemistry of both the grades. The load carrying ability of the IF–HSLA joint is found to be closer to that of IF–IF joint but significantly lower than that of HSLA–HSLA joint; this is because the location of failure for IF–HSLA and IF–IF joint is same, i.e., the HAZ/base metal interface at IF side, while that of HSLA–HSLA joint is the base metal of HSLA steel.

1. Introduction

Interstitial-free (IF) and high-strength low-alloy (HSLA) steels are among the most widely used grades in the automotive sector. They have gained widespread attention because of their high strength-to-weight ratio, excellent formability, and weldability (Ref 1). In the recent past, the joining of multi-material combinations of steels has gained tremendous attention involving steels with different microstructures and mechanical properties (Ref 2). Hence, for the auto-assembly structures involving the joining of dissimilar steels, inputs on the welding process parameters and mechanical behavior of the joints are essential. Chen et al. (Ref 3) reported that the joining of dissimilar steels is a challenging task due to the difference in chemical composition, microstructure, and physical properties. This results in the formation of asymmetrical weld nugget and shift in the solidification line. Aslanlar et al. (Ref 4) studied the welding parameters and mechanical properties of the spot welds on low-carbon steel sheets. It was reported that the load carrying capacity of the welded joints enhanced with the increase in welding current and time, which resulted in higher nugget size. Likewise, Pouranvari et al. (Ref 5) reported that the nugget size and mode of loading are the important factors

governing the mechanical performance of the low-carbon steel welds. Mukhopadhyay et al. (Ref 6) assessed the strength and microstructure of the spot welds on the IF steels. They showed that the strength of spot welds in the tensile shear configuration is higher than that of cross-tension configuration. It has been explained using von Mises criteria as the failure of joints in tensile shear and cross-tension configuration was governed by tensile stresses and shear stresses, respectively, at the micro-level. Hayat et al. (Ref 7) determined the load bearing capacity of the joints on the IF steel sheets of 0.8 mm thickness. They reported that the desired pullout failure was obtained for the welding current and time in the range of 7-9 kA and 25 cycles, respectively. Pouranvari and Marashi (Ref 8) studied the weldability and failure behavior for similar combinations of HSLA steel welds of 1.5 mm thickness. The minimum current to ensure weld joint failure in pullout mode was 9.5 kA. They proposed the model for determination of critical nugget diameter to ensure pullout failure mode. Khan et al. (Ref 9) reported the mechanical properties of the spot welds on HSLA steel sheets. It is presented that the failure mode is affected by joint strength, chemistry, and strain rate. Shome and Chatterjee (Ref 10) presented the effect of material properties on the contact resistance for the IF steel sheets. They showed that the contact resistance is affected by the strength of the sheet asperities and topography and yield strength of the material. Cho and Rhee (Ref 11) studied the crucial role of dynamic contact resistance (DCR) on nugget formation. They showed that during welding, the heat generation is dependent on dynamic contact resistance (DCR), which influences the melting of the mating surfaces and determines the nugget diameter. Most of the investigations on spot welding are primarily focused on the weldability, microstructural changes, and the mechanical properties for similar combinations of steel sheets. The mechanism of nugget formation for dissimilar combinations can be well understood by conducting the studies on the dynamic contact resistance. It is important to determine the effect of dynamic contact resistance (DCR) on nugget

Gorti Janardhan and **Krishna Dutta**, Department of Metallurgical and Materials Engineering, National Institute of Technology, Rourkela, India; and **Goutam Mukhopadhyay** and **Kaushal Kishore**, R&D and Scientific Services, Tata Steel Limited, Jamshedpur, India. Contact e-mail: g.janardhan@hotmail.com.

formation, growth, and expulsion for the dissimilar combination of steels, which is not well studied. Despite the available literature on resistance spot weldability of IF–IF and HSLA–HSLA steels, the effect of process parameters of resistance spot welding on DCR and subsequently its role on the quality of the welded joint has rarely been reported in the literature. Therefore, the current work has been carried out to establish the role of dynamic contact resistance on nugget formation and evaluate the mechanical behavior of the spot-welded joints of the two dissimilar grades, i.e., IF and HSLA steels, in different loading conditions. Further, to compare the performance of the dissimilar joint, joining of similar grades like IF–IF and HSLA–HSLA steels has been considered. In addition, microstructural examination, determination of hardness profiles, location of failure, and analysis of fractographic features have been carried out in detail.

2. Experimental Procedure

2.1 Material Selection and Preparation of Spot-Welded Specimens

Bare interstitial-free (IF) and high-strength low-alloy (HSLA) steel sheets of 1.2 mm thickness were selected for the present investigation. The chemical analysis was carried out using an x-ray fluorescence spectrometer (Model: Ametek Spectrolab, USA). The chemical compositions of the IF and HSLA steels are given in Table 1.

Specimens were cut for examining the microstructures along longitudinal as well as transverse directions of the sheets. These were prepared according to standard metallography procedure, and microstructures were studied by optical microscopy (Model: Leica DM6000M, Germany). The average grain size of the steels was determined based on the linear intercept method ASTM E112 (Ref 12). IF steel shows predominately equiaxed ferrite grains of size 23 ± 1 μm, while HSLA steel shows finer ferrite grains with an average size of 10 ± 0.48 μm. The tensile tests of as-received steel sheets were carried out according to ASTM standard E8M-16 (Ref 13) using a servo-electric universal testing machine (Model: Instron 5582, UK). Table 2 depicts the tensile properties of the examined steels. Figure 1 shows the engineering stress versus strain curves for the IF and HSLA steel sheets. The yield and tensile strength of the IF steel were lower than those of the HSLA steel, while the total elongation of IF steel was higher as

expected. The higher strength of HSLA steel was attributed to the presence of higher C, Mn, and Nb apart from its finer grain size. The HSLA steels containing small amounts of microalloying elements such as Nb or Ti are produced by controlled thermomechanical rolling with accelerated cooling. Niobium (Nb) plays a vital role in precipitation hardening, retarding the recrystallization temperature of austenite, consequently promoting the grain refinement and increasing the yield strength (Ref 14, 15).

Spot welding was carried out on a pedestal-type inverter-based 150 kVA medium-frequency direct current machine (Model: Mechelonic engineers, India). Figure 2(a) shows the welding parameters considered for the current study. The electrodes used in the present investigation were made up of copper–chromium–zirconium alloy (Cu-Cr-Zr) of Resistance Welder Manufacturers Association (RWMA) class-II. The electrodes were of truncated conical shape with cap diameter and an electrode tip diameter of 16 and 6 mm. The current was measured using the Rogowski coil placed on the upper arm of the electrode (Fig. 2b). The voltage data were acquired by attaching alligator clips on the electrodes, as shown in Fig. 2(b). A weld checker (Model: 370B, Miyachi, China) was employed for digital recording of the voltage and current values. The values of contact resistance were estimated following Ohm's law, respectively. Two types of weld joints
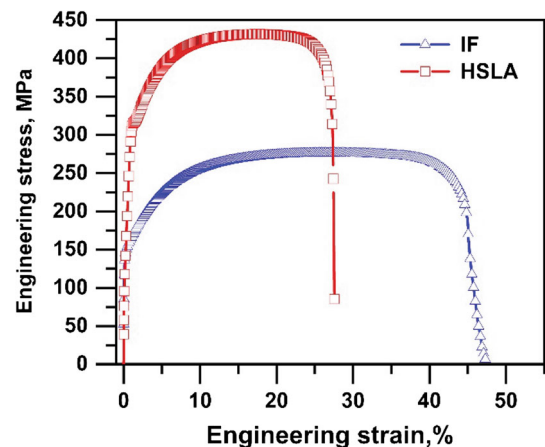

Fig. 1 Engineering stress–strain curves of IF and HSLA steels

Table 1 Chemical composition (wt.%) of the investigated HSLA and IF steel

Steels	C	Mn	S	P	Si	Al	Cr	Ni	Ti	Nb	N	Fe
HSLA	0.039	1.45	0.006	0.023	0.007	0.042	0.018	0.016	0.001	0.012	0.0019	Bal.
IF	0.002	0.10	0.008	0.010	0.002	0.073	0.012	0.016	0.054	0.001	0.0024	Bal.

Table 2 Tensile properties of HSLA and IF steels

Steels	YS, MPa	UTS, MPa	% Uniform elongation	% Total elongation
HSLA	310 ± 3.05	432 ± 4	14.08 ± 3	26.19 ± 1.5
IF	144 ± 2.08	275 ± 5	27.25 ± 2.5	49.46 ± 2
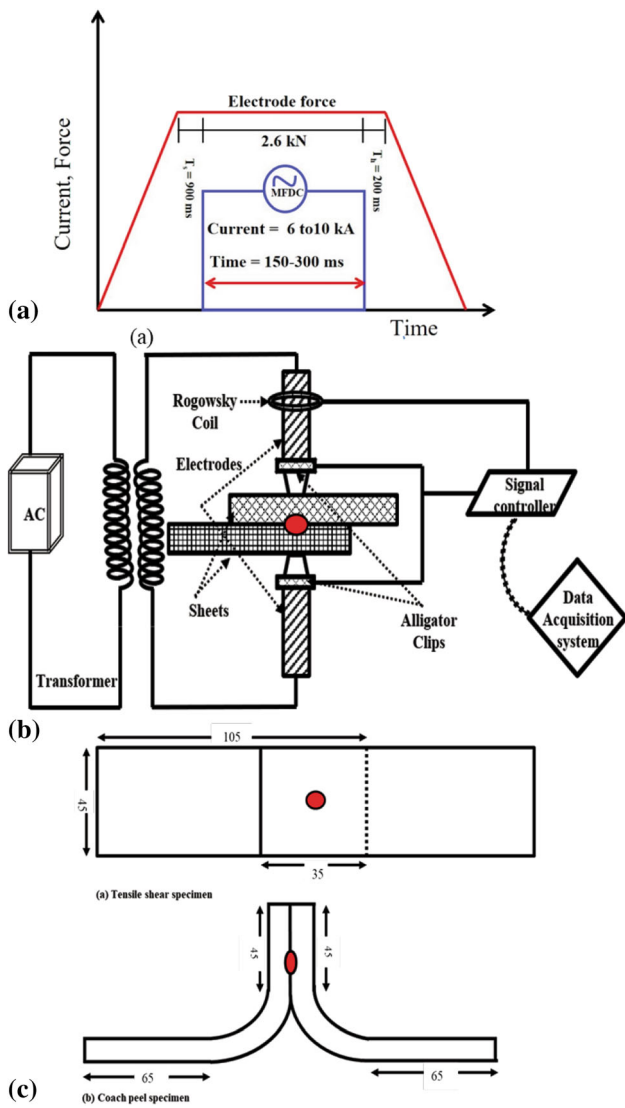
Fig. 2 (a) Schematic of spot welding parameters, (b) schematic of resistance spot welding process, and (c) schematic configurations of the tensile shear (TS) and coach peel (CP) specimens (all dimensions are in mm)

were designed following BS1140:1993 standard with geometry and dimensions of the specimens, as shown in Fig. 2(c).

2.2 Characterization of Spot Welds

The resistance spot-welded specimens were cut using a slow-speed disk cutter marginally above the weld centerline, and the specimens were prepared according to the standard metallography procedure. A stereo microscope (Model: Leica 205A, Germany) was used to observe the macrostructure of the weld cross section and measure the nugget diameters at different welding parameters. The microstructure of the spot welds at different welding parameters was examined using an optical microscope (Model: Leica DM6000M, Germany) and a scanning electron microscope (Model: FEI Nova NanoSEM 430, USA). Vickers microhardness tester (Model: EMCO DuraScan 20GS, Austria) was used to determine the microhardness profile along the various zones of the spot-welded joints using a load of 100 gf and dwell time of 15 s. The load

bearing capacity of the welds was determined with the help of a servo-electric universal testing machine (Model: Instron 5582, UK) at a crosshead speed of 5 mm/min using tensile shear and coach peel configurations as shown in Fig. 2(c). These tests were repeated at least three times for identical specimens welded at a particular process parameter, and the averages, as well as the standard deviation of three measurements, have been reported. Specimens were cut from the failed locations of the joints to examine the microstructure to investigate the initiation and propagation of cracks in different modes of loading. Fractographic examination of the failed joints was carried out using the scanning electron microscope (SEM) (Model: Zeiss, Supra 25, Germany) to identify the modes of failure.

3. Results and Discussion

3.1 Dynamic Contact Resistance Behavior of the Spot-Welded Joint

The variations in contact resistance during the spot welding of IF and HSLA steel sheets at different welding currents, at a constant welding time of 300 ms and electrode force of 2.6 kN, are shown in Fig. 3(a). For a particular current value, during the initial upslope time, the initial contact resistance falls rapidly to a minimum value (referred as R_{min}); after that, the contact resistance increases and finally reaches a higher resistance value denoted as the β peak. (This β peak manifests the shift from nugget formation to growth stage.) After the β peak, the contact resistance gradually decreases and remains consistent until the end of welding, as shown in Fig. 3(a). The initial sudden reduction in contact resistance values with the increase in time is related to the electrical and mechanical collapse of surface films asperities because of electrode voltage and electrode force, respectively, as reported by Wan et al. (Ref 16). After the breakdown of surface asperities, contact is established between the surfaces and, then, enlargement of the contact area takes place. The heat generated is mainly concentrated at the interface of the two sheets. Therefore, the temperature of the corresponding positions increases significantly. At the same time, the resistivity of the bulk material increases with temperature. This explains the gradual increase in contact resistance value after the R_{min} point. The nature of the contact resistance curves is in good agreement with the work of Rao et al. (Ref 17). They studied the effect of welding parameters on the DCR for the IF steel-welded joints. Table 3 shows the values of the nugget diameter, minimum contact resistance (R_{min}), dynamic contact resistance (DCR), and β peak at different welding parameters.

It is observed that the nugget formed at 6 kA exhibited the highest β peak and the maximum R_{min} value, which lead to the lowest nugget diameter as shown in Table 3. Moreover, it could be observed that the size of the nugget increases with an increase in welding current until 9 kA as the DCR value (R_{min} or β peak) reduces gradually. This gradual decrease in contact resistance values with the increase in current is attributed to the pronounced collapse of the sheet surface and asperity softening as stated for spot-welded IF steels as discussed in Ref 10. The contact resistance curve corresponding to 10 kA welding current shows further sudden drop after the β peak (as shown in Fig. 3b). This drop indicates the expulsion of the fused metal
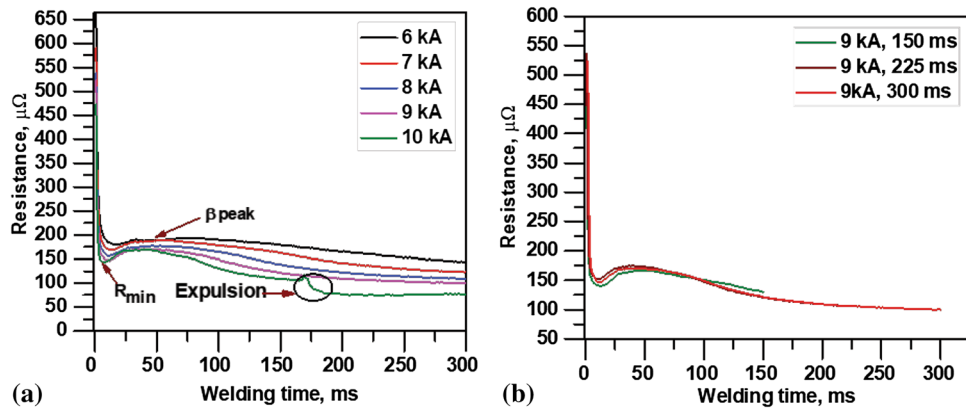
Fig. 3 (a) DCR curves at different welding parameters at constant welding time of 300 ms and electrode force of 2.6 kN

Table 3 Salient features of contact resistance plots at different welding process parameters

Sl. no.	Weld current, kA	Electrode force, kN	Weld time, ms	Mean DCR, μΩ	Nugget diameter, mm	Minimum contact resistance, R_{min}	β peak Weld time, ms	β peak Resistance, μΩ
1	6	2.6	300	176.7	3.46	179.3	45	193
2	7	2.6	300	160.2	4.84	167.7	55	189
3	8	2.6	300	143.82	5.64	159.71	77	173
4	9	2.6	150	154	5.52	141	42	173
5	9	2.6	225	141.95	6.35	153	42	166
6	9	2.6	300	131.4	6.63	146.6	59	168
7	10	2.6	300	113.8	6.3	143.67	43	158

from the weld pool. Because of the expulsion, the nugget diameter corresponding to this current reduces and hence undesirable. Figure 3(b) shows the variations in contact resistance characteristics of IF and HSLA spot-welded joints at different welding times, at a constant current of 9 kA and constant electrode force of 2.6 kN. It shows that as the welding time increases, the mean DCR value decreases (as illustrated in Table 2); it dropped from 154 to 131 μΩ, i.e., by 14% with the increase in welding time from 150 to 300 ms. This could be attributed to the dominating effect of the interfacial contact resistance over the bulk resistance of the material; interfacial contact resistance between the sheets is dependent upon asperity softening phenomena as presented by Wan et al. (Ref 16).

Figure 4 shows the variation of nugget diameter (D) with the mean dynamic contact resistance (DCR) values within the adequate range. The nugget diameter increases with the decrease in mean dynamic contact resistance. This is in good agreement with the relationship between nugget diameter and mean DCR for Q235 steel sheets, as reported by Luo et al. (Ref 18). In present IF–HSLA combination of steel joints, the linear best fit equation with R^2 value of 0.90 is useful to describe the relationship between the nugget diameter and dynamic contact resistance as follows:

$$D = -0.08106 \times DCR + 17.673. \qquad \text{(Eq 1)}$$

As the welding current is increased, the cross-sectional area for the passage of welding current is progressively increased due to the successive melting at contact interfaces. The mechanical collapse caused by material softening and electrode
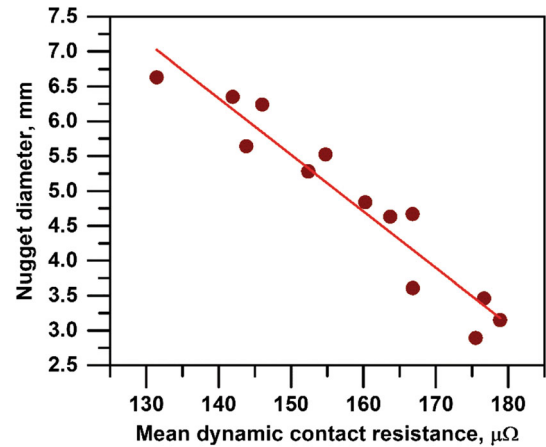

Fig. 4 Variation of nugget diameter with mean dynamic contact resistance (DCR) for IF–HSLA joints

pressure would shorten the current flow path. These two effects lead to a reduction in the dynamic contact resistance and an increase in nugget diameter. Thus, the characteristics of DCR curves obtained during the welding are proved to be a useful indication to assess nugget development.

3.2 Macro- and Microstructural Characterization

A typical macrograph of the cross section of the spot-welded joint is shown in Fig. 5. The macrostructure reveals three
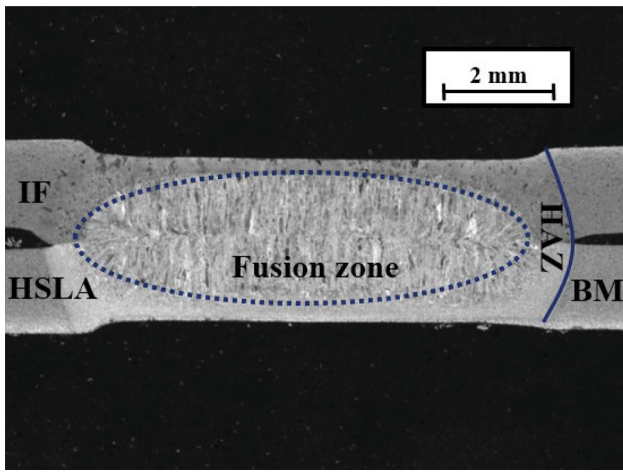
Fig. 5 Typical macrostructure of IF–HSLA spot-welded joints at 9 kA, 225 ms, 2.6 kN

distinct zones of RSW, namely fusion zone (FZ), heat-affected zone (HAZ), and base metal (BM).

The optical micrographs of FZ and HAZ are shown in Fig. 6(a), (b), (c), (d), (e), and (f), whereas the SEM images of the three different zones are presented in Fig. 7(a), (b), (c), (d), (e), (f), (g), and (h). The microstructure of the fusion zone (FZ) of IF/HSLA dissimilar metal weld consists of columnar grains as shown in Fig. 6(a) The microstructure of FZ reveals martensite and some acicular as well as Widmanstatten ferrites as shown in Fig. 6(b) and 7(a), (b). The very high cooling rate of the order of 10^4 °C/s due to the quenching effect offered by the water-cooled copper electrodes and very short weld time of 0.2-0.6 s lead to the formation of martensite in the fusion zone as shown by Bhadeshia and Honeycombe (Ref 19). The optical and SEM micrographs of the HAZ of the IF steel are shown in Fig. 6(c), (d) and 7(c). The HAZ as shown in Fig. 6(c) and (d) reveals relatively fine ferrite grains near the FZ (as indicated by arrow/boundary line in Fig. 6a) followed by larger elongated ferrite grains next to it away from the FZ in the direction of heat flow. This could be attributed to the annealing effect induced during the thermal cycle of the welding as reported in Ref 20. The elongated grains are formed in the regions where the attained peak temperature was above Ac_3; this region experiences a higher temperature for the longest period of time as shown in Ref 20. This leads to the formation and growth of austenite grains resulting in larger ferrite grains during cooling. The microstructure of IF steel mostly consists of ferrite grains due to the very low level of carbon (refer Fig. 7d). The HAZ of HSLA steel shows a different microstructural feature as compared to IF steel, as shown in Fig. 6(e), (f) and 7(e), (f), (g). The region near to FZ reveals coarse-grained heat-affected zone (CGHAZ), whereas fine-grained heat-affected zone (FGHAZ) is formed away from it as shown in Fig. 6(e), (f) and 7(e), (f). The microstructure of CGHAZ of the HSLA steel consists of coarse martensite with some ferrite grains as shown in Fig. 7(e). The FGHAZ of the HSLA steel shows finer martensite with some ferrite grains as shown in Fig. 7(f). The temperatures in FGHAZ and CGHAZ are well above Ac_3, resulting in a fully austenitized structure during welding. The transitional region between the base metal and the HAZ is the intercritical heat-affected zone (ICHAZ) in the case of HSLA steel. In ICHAZ, both ferrite and martensite are observed as

shown in Fig. 7(g). This is because temperature attained in ICHAZ is between Ac_1 and Ac_3, as stated in Ref 21. In ICHAZ, the martensite content gradually increases from the base metal side to the fusion zone as the temperature increases towards fusion zone direction; Fig. 7(h) represents microstructure of the micro-alloyed HSLA steel, which consists of fine ferrite and cementite at its boundaries as shown in Fig. 7(h) depending upon its alloying element and thermomechanical processing. The precipitates present in the HSLA steel is characterized as (FeMn)C type as confirmed by the EDS analysis. Owing to higher Mn content in the investigated steel, the MnC precipitates are formed predominantly. Manganese is a solid solution strengthening element as well as austenite stabilizer. It plays a vital role in reducing the austenite to ferrite transformation temperature, consequently promoting refinement of ferrite grains (Ref 14, 15). The presence of numerous precipitates in the HSLA steel with similar chemical composition has been reported by Khan et al. (Ref 21).

### 3.3 Hardness Profiles Along the Spot Welds

Figure 8(a) shows the microhardness profile for the IF–HSLA dissimilar combination of the spot-welded joint. The microhardness value is the lowest (93 HV) on the BM region of the IF steel. The microhardness profile in the IF steel side of the weld sharply increases from BM to FZ through HAZ. In IF steel side, there is an increase in hardness in HAZ compared to BM.

The microhardness in the BM region of HSLA steel is higher (162 HV) as compared to the IF steel due to the finer ferrite grains as discussed in the earlier section. In contrast to the continuous increase in hardness profile at the IF steel side weld, the profile at the HSLA steel side shows a sharp increase in hardness from BM to HAZ and then a drop at the FZ. The sharp increase in hardness from BM to HAZ is because of the microstructural change from ferrite to martensite and then the drop in the hardness in FZ is because of the microstructural differences due to its mixed and homogenized chemical composition of both the dissimilar grades, i.e., IF steel and HSLA steel.

The hardness at the FZ of the weld is approximately consistent in nature with an average hardness of 270 HV at the HSLA steel side and 267 HV in the IF steel side; the marginal difference is attributed to the difference in the chemistry of both the grades. The hardness in the HAZ region of HSLA steel (357 HV) is significantly greater than that of the IF steel (157 HV). This is because of the formation of martensite in the CGHAZ and FGHAZ regions of HSLA steel and ferrites in the HAZ of IF steel because of their difference in chemistry. The microhardness values for both IF–IF and HSLA–HSLA weld joints at constant welding parameters are shown in Fig. 8(b). The hardness at the fusion zone of the dissimilar HSLA–IF joint lies in between that of fusion zone of similar HSLA–HSLA or IF–IF joints because of the homogenization of the chemistry of both the grades. The obtained microhardness profiles are in good agreement with the results of Khan et al. (Ref 21), Rathbun et al. (Ref 22), Long and Khanna (Ref 23), and Pouranvari and Marashi (Ref 8).

3.4 Influence of Welding Current on Nugget Diameter

Figure 9 shows the influence of welding current on the nugget diameter. It is observed that the nugget diameter increases with an increase in welding current. This increase in
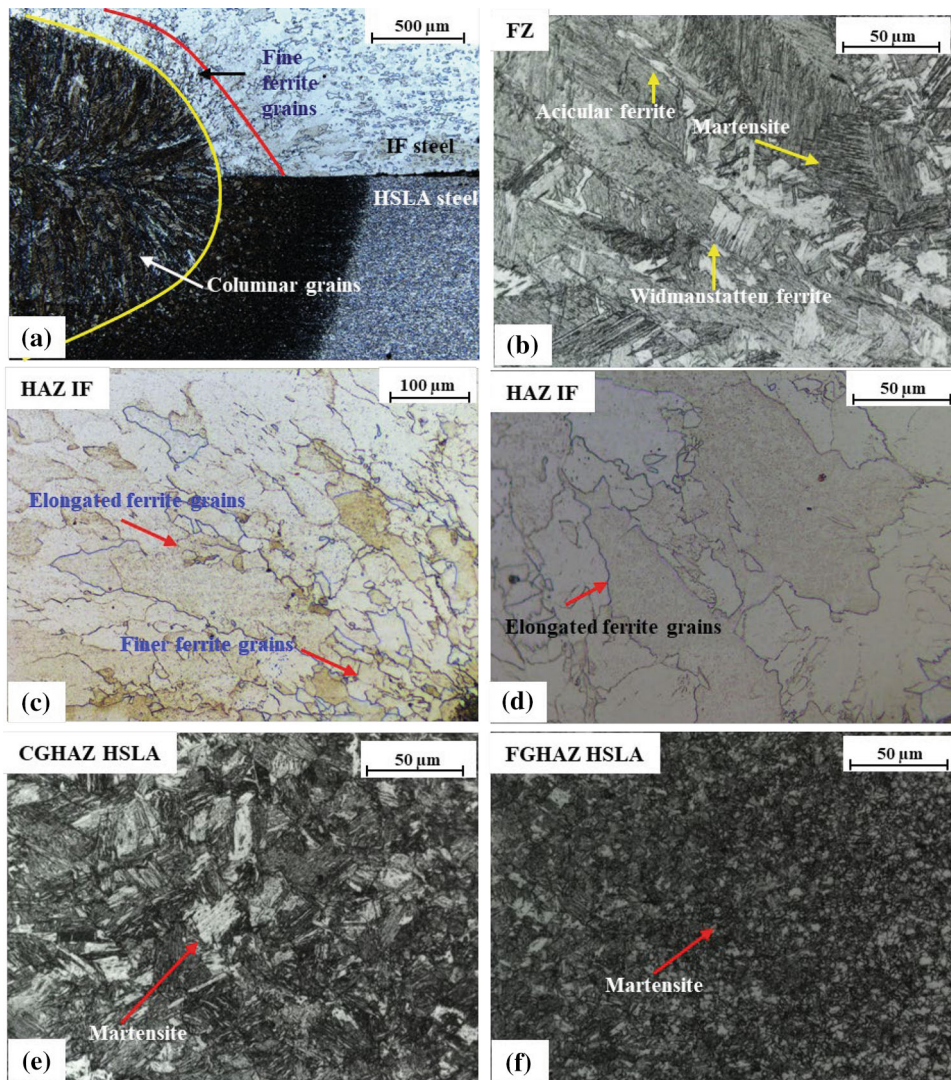
Fig. 6 Macro- and microstructures of the spot-welded IF–HSLA steels: (a) macrostructure, (b) fusion zone, (c, d) heat-affected zone (HAZ) of IF steel, (e) coarse-grained heat-affected zone (CGHAZ) of HSLA steel, and (f) fine-grained heat-affected zone (FGHAZ) of HSLA steel, respectively

nugget size was because of the increase in heat input, which increases with an increase in welding current. The maximum weld nugget diameter is observed at 9 kA welding current, 300 ms weld time, and 2.6 kN electrode force. Expulsion of molten metal from the weld pool takes place at 10 kA welding current, 225 ms weld time, and 2.6 kN electrode (refer Fig. 9). Expulsion is undesirable as it leads to a reduction in the nugget size, causing the formation of defects such as shrinkage voids, porosity, and cavities in the weld nugget.

3.5 Mechanical Properties of the Spot-Welded Joints

Typical load–displacement curves for the tensile shear samples at varying welding current from 6 to 10 kA at a constant welding time of 300 ms and electrode force of 2.6 kN are shown in Fig. 10(a). It could be observed that as the welding current increases from 6 to 10 kA, both the peak load

and the corresponding elongation of the spot-welded joints increase simultaneously up to 9 kA and consequently the energy absorbed during the failure increases. However, at 10 kA the peak load and the absorbed energy of the joint reduced due to the expulsion of molten metal. As already mentioned in "Influence of Welding Current on Nugget Diameter," expulsion causes a reduction in the nugget size, which reduces the load carrying ability of the TS specimens.

The load versus displacement plots of the coach peel samples at varying welding currents from 6 to 10 kA, at constant welding time of 300 ms and electrode force of 2.6 kN, are shown in Fig. 10(b). Here also, the nature of the load carrying ability is similar to that of the TS samples. CP samples exhibit lower load carrying ability and energy absorption compared to that of TS samples. A similar observation has also been reported by researchers in Ref 8. This is attributed to the complex state of stress in CP configuration as it involves
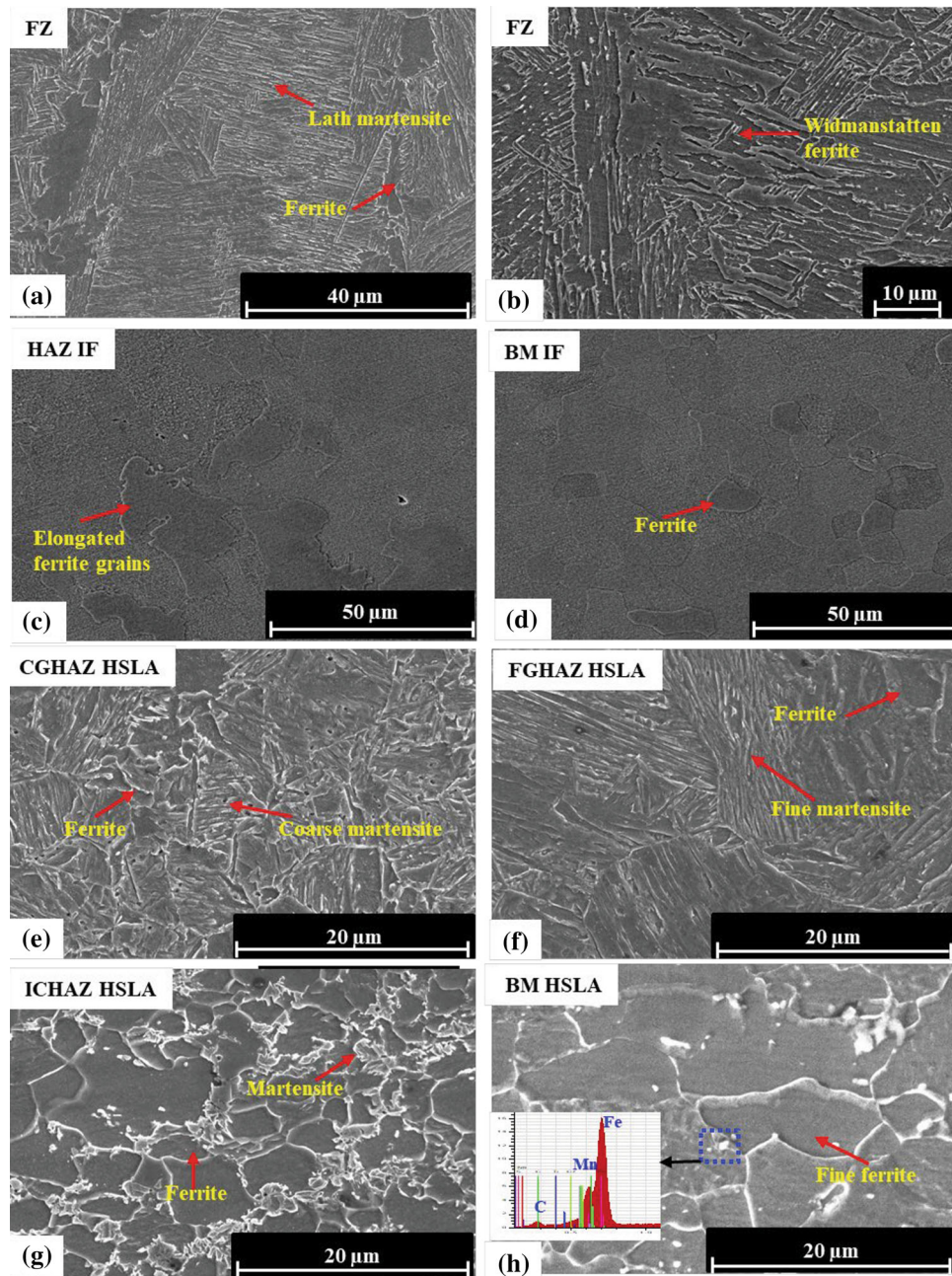
Fig. 7 SEM micrographs of IF–HSLA joints: (a, b) fusion zone (FZ), (c) heat-affected zone (HAZ), (d) base metal (BM) of IF steel, (e) coarse-grained heat-affected zone (CGHAZ), (f) fine-grained heat-affected zone (FGHAZ), (g) intercritical heat-affected zone (ICHAZ), (h) base metal of HSLA steel

bending moment induced due to tensile loading. During the testing of CP samples, the crack initiation at the weld nugget takes place entirely focusing at a single point or very smaller area. Therefore, the load carrying ability of CP samples is lower than that of TS specimens. The reduction in load carrying ability at 10 kA for the CP specimens is because of the expulsion at the joint due to very high heat input. During expulsion, samples experience excessive electrode indentation and reduction in the size of the weld nugget, which in turn reduces the mechanical performance of the joint. Figure 11 shows the effect of the nugget diameter on the load carrying ability and energy absorption capacity of the spot welds of TS and CP specimens. It was observed that the load carrying ability and energy absorption of the spot welds increased with an increase in weld nugget diameter within the experimental range for both CP and TS test specimens. The maximum load and energy absorption by the spot welds in the TS configuration were found to be 8.3 kN and 30 J, respectively, at welding
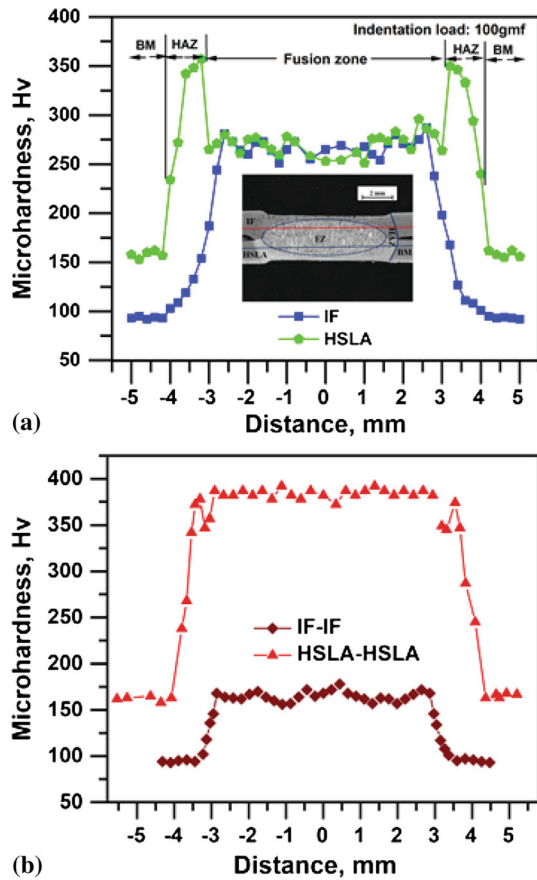
Fig. 8 (a) Hardness profiles across the spot-welded regions of IF–HSLA joints, (b) refers to hardness profiles of the IF–IF and HSLA–HSLA joints
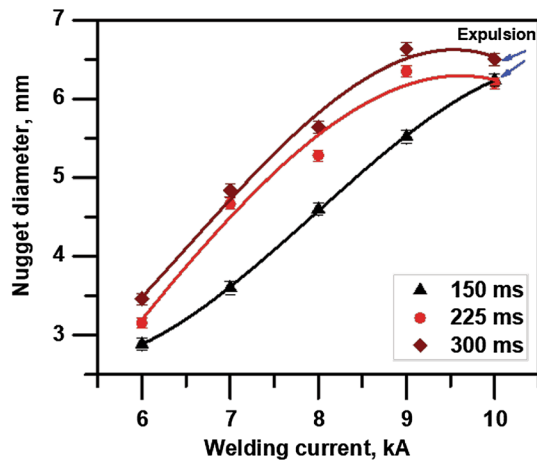
Fig. 9 Variation of nugget diameter with the welding current

current, welding time, and electrode force of 9 kA, 300 ms, and 2.6 kN, respectively. It was interesting to note that the trends for the variation of load carrying ability and energy absorption of the spot welds with nugget diameter have greater scatter in CP specimens as compared to that of TS specimens. The load carrying ability of the CP samples is governed by the thickness of the sheet rather than the nugget diameter as reported in Ref 24. The load carrying ability of the TS specimens is lowest at a current of 6 kA where the nugget diameter was found to be lowest even less than that of 10 kA weld current (refer Fig. 11). In case of TS specimens at 6 kA, interfacial failure occurs, unlike that of CP specimens where pullout failure occurred at 6 kA. This is because of the difference in the mode of loading. Figure 12 shows the comparison of load carrying capacity of TS specimens for the similar and dissimilar joints of IF and HSLA steels. The load carrying ability of the IF–HSLA joint is found to be closer to that of IF–IF joint but significantly lower (almost half) than that of HSLA–HSLA joint; this is because the location of failure for IF–HSLA and IF–IF joint is same, i.e., the HAZ/base metal interface at IF side (as discussed in the next section), while that of HSLA–HSLA joint is the base metal of HSLA steel. The marginal higher strength of the IF–HSLA joint compared to that of the IF–IF joint is because of its marginally higher nugget diameter (6.35 mm) than that (6.21 mm) of IF–IF joint.

3.6 Post-failure Examination of Spot-Welded Joints

To study the fractographic features, SEM images were taken at the location of failures. Figure 13 shows the SEM micrograph of the fractured surface of the weld nugget failed under pullout mode. Shear dimples were observed in the region near to the failure location. This was because of the shearing action offered by the tearing of the base metal after the crack initiated at the HAZ/base metal interface. These elongated dimples suggest predominantly tensile stress during the pullout failure of the TS specimens.

The cross-sectional microstructures of the failed weld nuggets were examined to identify the location of failure. Figure 14(a) and (b) represents the cross-sectional view of the failed spot-welded TS specimen of the IF–HSLA joint. It was observed that the failure of the joints initiated on the IF steel side. Significant necking associated with grain flow occurred in the base metal due to a higher degree of plastic deformation. The failure initiated at the HAZ/base metal interface of the IF steel side because of its lower hardness and strength compared to that of other locations. Therefore, the location of the failure of spot welds is governed by the strength and hardness values in different zones of the weld. Figure 14(c) shows the cross-sectional of a failed TS specimen of IF–IF joint which exhibits the location of failure at the HAZ/base metal interface similar to that of the IF–HSLA joint. On the other hand, the location of failure of the TS specimen of the HSLA–HSLA joint as shown in Fig. 14(d) is base metal. This is attributed to the lowest
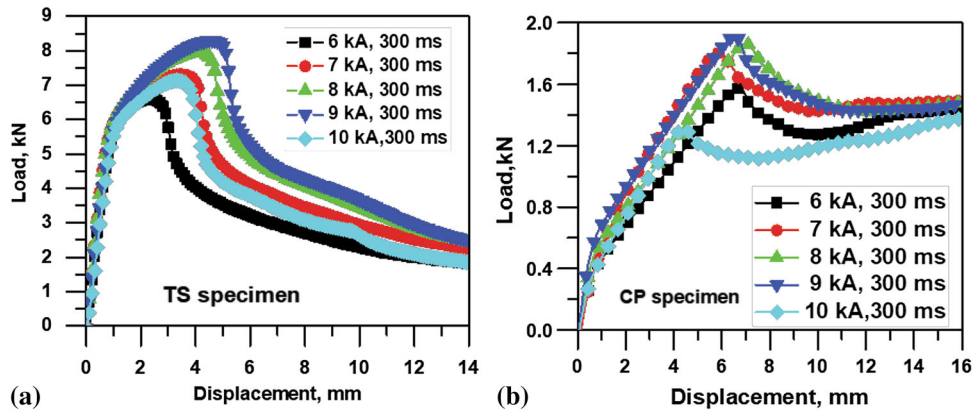
Fig. 10 Typical load–displacement curves at varying welding currents: (a) refers to tensile shear specimens; (b) refers to coach peel specimens
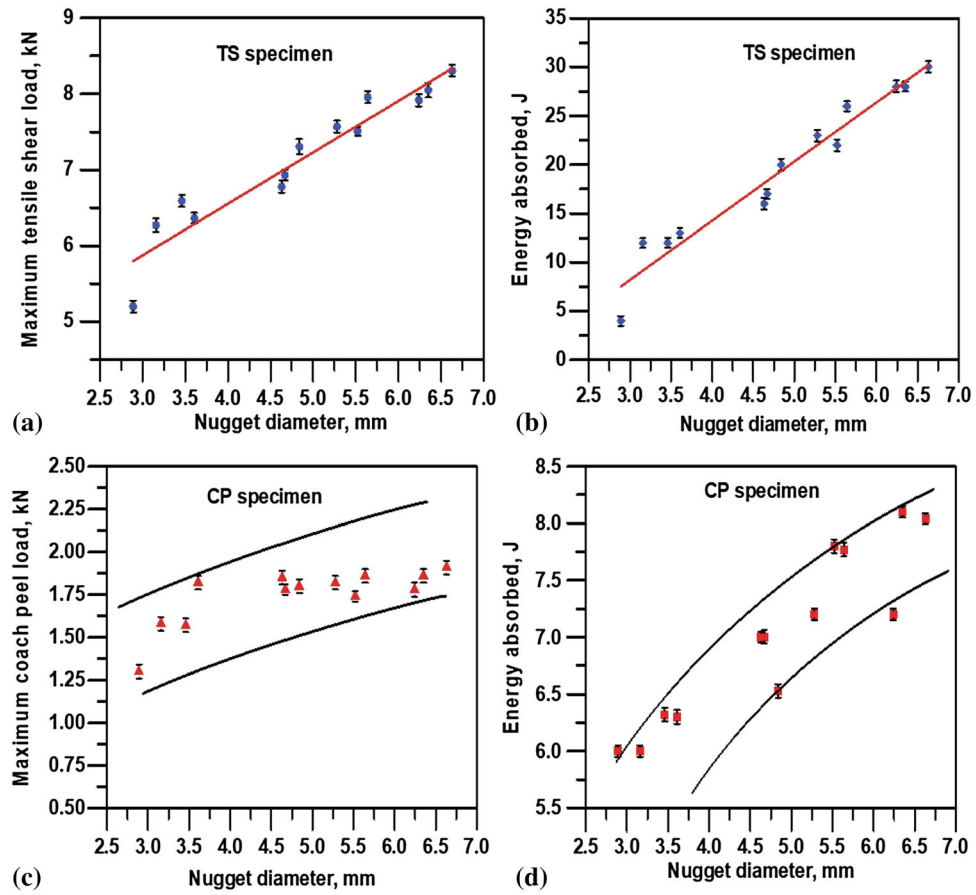

Fig. 11 Effect of the nugget diameter on the load carrying ability and energy absorption capacity: (a, b) refers to the tensile shear (TS) specimens; and (c, d) refers to coach peel (CP) specimens
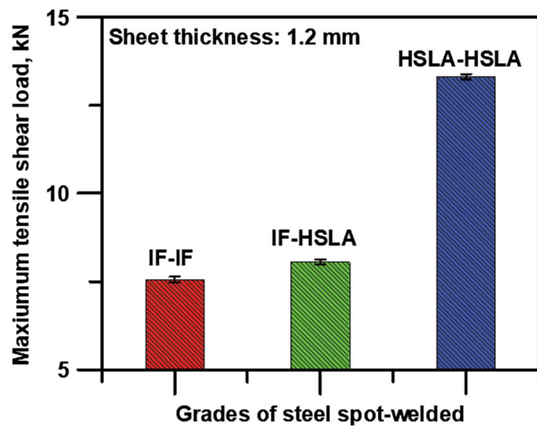
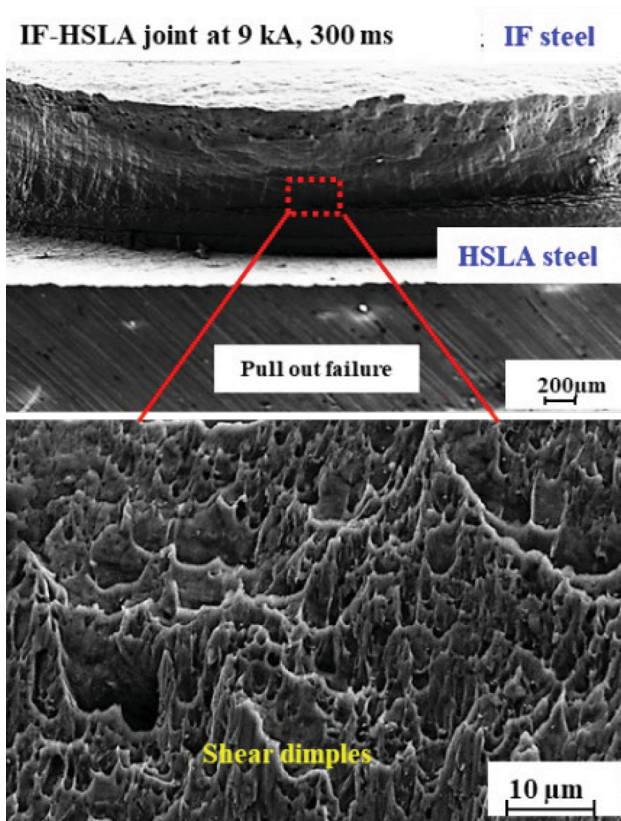**Fig. 12** Comparison of load carrying capacity of the spot welds

**Fig. 13** Fractography of pullout mode during tensile shear test

hardness at the base metal zone in the case of the HSLA–HSLA joint.

It is noteworthy to mention that the hardness of the failure location of the IF–HSLA combination on the IF side is nearly same as that of the hardness of the failed location of the IF–IF welds and significantly lesser than the hardness of failed location of HSLA–HSLA welds. Therefore, the load carrying capacity of the IF–HSLA joints is closer to IF–IF joints and half times that of HSLA–HSLA joints.

4. Conclusions

The following are the major conclusions of the present study:

- Weldability study of IF and HSLA steel sheets of thickness 1.2 mm reveals that the maximum load carrying ability of the spot-welded joint in both tensile shear and coach peel configurations is obtained at a welding current, time, and electrode force of 9 kA, 300 ms, and 2.6 kN, respectively. The load carrying ability and energy absorption of the spot welds under both tensile shear and coach peel loading conditions increased with the increase in nugget diameter.
- The dynamic contact resistance (DCR), during welding of the sheets, controls the total heat input and thereby the nugget formation and growth at different welding parameters. An increase in welding current resulted in reduction in the mean DCR value and hence an increase in the nugget diameter.
- The hardness of the fusion zone of the dissimilar IF–HSLA joint shows a drop from that of HAZ and lies in between that of fusion zone of similar HSLA–HSLA and IF–IF joints because of the mixing and homogenization of the chemistry of both the grades. The failure occurs from the lowest hardness zone among the various zones, i.e., fusion zone, HAZ, or base metal, of the weld joint.
- The load carrying ability of dissimilar IF–HSLA steel joint is measured to be closer to that of IF–IF joint and significantly lower than that of HSLA–HSLA joint; this is because the location of failure for both IF–HSLA joint and IF–IF joint is similar, i.e., HAZ/base metal interface of IF steel, while that of HSLA–HSLA joint is base metal having higher strength.
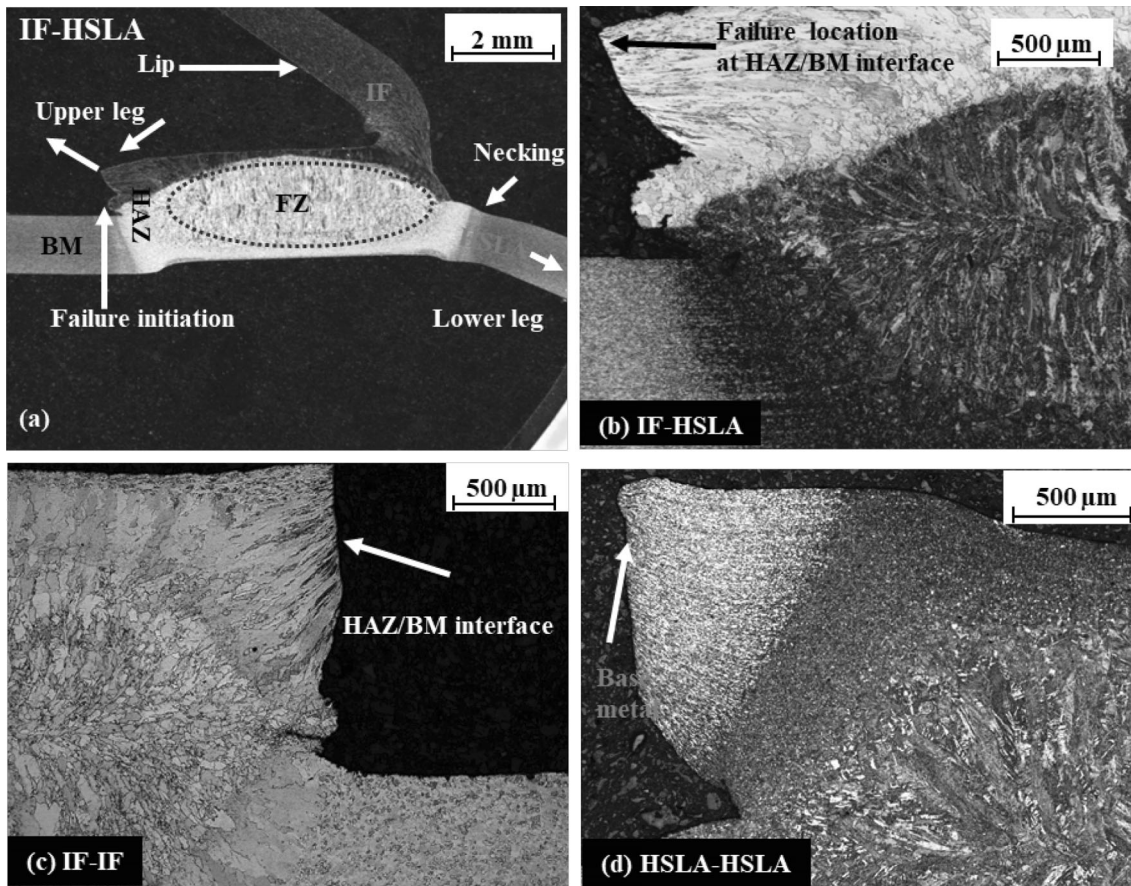
Fig. 14 Typical cross sections of the failed spot welds after the tensile shear test: (a, b) failed spot weld of IF–HSLA joint, (c) failed spot weld of IF–IF joint, (d) failed spot weld of HSLA–HSLA joint

References

1. D.K. Matalock, J.G. Speer, E. De Moor, and P.J. Gibbs, Recent Developments in Advanced High Strength Steel Sheets for Automotive Applications: An Overview, *Jestech*, 2012, **15**, p 1–12
2. M. Pouranvari and S.P.H. Marashi, Critical Review of Automotive Steels Spot Welding: Process, Structure and Properties, *Sci. Technol. Weld. Join.*, 2013, **18**, p 361–403
3. N. Chen, P.H. Carlson, B.E. Sigler, and M. Wang, Fracture Mechanisms of Al/Steel Resistance Spot Welds in Coach Peel and Cross Tension Testing, *J. Mater. Process. Technol.*, 2018, **252**, p 348–361
4. S. Aslanlar, A. Ogur, U. Ozsarac, and E. Ilhan, Welding Time Effect on the Mechanical Properties of Automotive Steels Electrical Resistance Spot Welding, *Mater. Des.*, 2008, **29**, p 1427–1431
5. M. Pouranvari, S. Sobhani, and F. Goodarazi, Resistance Spot Welding of MS1200 Martensitic Advanced High Strength Steel: Microstructure—Properties Relationship, *J. Manuf. Proc.*, 2018, **31**, p 867–874
6. G. Mukhopadhyay, S. Bhattacharya, and K.K. Ray, Strength Assessment of Spot-Welded Interstitial Free Steels, *J. Mater. Process. Technol.*, 2009, **209**, p 1995–2007
7. F. Hayat, B. Demir, M. Acarer, and S. Aslanar, Effect of the Weld Time and Weld Current on the Mechanical Properties of the Resistance Spot-Welded IF (DIN EN 10130-1999) Steel, *Kovove Mater.*, 2009, **47**, p 11–17
8. M. Pouranvari and S.P.H. Marashi, Factors Affecting Mechanical Properties of Resistance Spot Welds, *Mater. Sci. Technol.*, 2010, **26**, p 1137–1144
9. M.I. Khan, M.L. Kuntz, and Y. Zhou, Effects of Weld Microstructure on the Static and Impact Performance of Resistance Spot Welded Joints in Advanced High Strength Steels, *Sci. Technol. Join.*, 2008, **13**, p 294–304
10. M. Shome and S. Chatterjee, Effect of Material Properties on Contact Resistance and Nugget Size during Spot Welding during Low Carbon Coated Steel, *ISIJ Int.*, 2009, **49**, p 1384–1391
11. Y. Cho and S. Rhee, Experimental Study of Nugget Formation in Resistance Spot Welding, *Weld. J.*, 2003, **82**, p 195S–201S
12. ASTM E112-12, *Standard Test Methods for Determining Average Grain Size*, ASTM International, West Conshohocken, 2012
13. ASTM E8/E8M/16a, *Standard Test Methods for Tension Testing of Metallic Materials*, ASTM International, West Conshohocken, 2016
14. R. Rana and S.B. Singh, *Automotive Steels: Design, Metallurgy, Processing and Applications*, 1st ed., Woodhead Publishing, Cambridge, 2016
15. D. Bhattacharya and S. Misra, Development of Microalloyed Steels through Thin Slab Casting and Rolling (TSCR) Route, *Trans. Indian Inst. Met.*, 2017, **70**, p 1647–1659
16. X. Wan, Y. Wang, and D. Zhao, Qaulity Monitoring Based on Dynamic Resistance and Principal Component Analysis in Small Scale Resistance Spot Welding Process, *Int. J. Adv. Manuf. Technol.*, 2016, **86**, p 3443–3451
17. S.S. Rao, R. Chhibber, K.S. Arora, and M. Shome, Resistance Spot Welding of Galvannealed High Strength Interstitial Free Steel, *J. Mater. Process. Technol.*, 2017, **246**, p 252–261

18. Y. Luo, W. Rui, X. Xie, and Y. Zhu, Study on the Nugget Growth in Single-Phase AC Resistance Spot Welding Based on the Calculation of Dynamic Resistance, *J. Mater. Process. Technol.*, 2016, **229**, p 492–500

19. H. Bhadeshia and R. Honeycombe, *Steels: Microstructure and Properties*, 4th ed., Butterworth-Heinemann, New York, 2006

20. S. Salim Beni, M. Atapour, M.R. Salmani, and R. Ashiri, Resistance Spot Welding Metallurgy of Thin Sheets of Zinc-Coated Interstitial-Free Steel, *Metall. Mater. Trans. A*, 2019, **50**, p 2218–2234

21. M.S. Khan, S.D. Bhole, D.L. Chen, E. Biro, G. Boudreau, and J. van Deventer, Welding Behaviour, Microstructure and Mechanical Properties of Dissimilar Resistance Spot Welds Between Galvannealed HSLA350 and DP600 Steels, *Sci. Technol. Join.*, 2009, **14**, p 616–625

22. R.W. Rathbun, D.K. Matlock, and J.G. Speer, Fatigue Behavior of Spot Welded High-Strength Sheet Steels, *Weld. J.*, 2003, **82**, p 207–218

23. X. Long and S.K. Khanna, Fatigue Properties and Failure Characterization of Spot Welded High Strength Steel Sheet, *Int. J. Fatigue*, 2007, **29**, p 879–886

24. L. Han, M. Thornton, D. Boomer, and M. Shergold, A Correlation Study of Mechanical Strength of Resistance Spot Welding of AA5754 Aluminium Alloy, *J. Mater. Process. Technol.*, 2011, **211**, p 513–521